New Journal of Physics
The open–access journal for physics

Charge change-induced beam losses under dynamic vacuum conditions in ring accelerators

C Omet[1,3,4], **P Spiller**[1], **J Stadlmann**[1] **and D H H Hoffmann**[1,2]

[1] GSI Darmstadt, Planckstr. 1, 64291 Darmstadt, Germany
[2] Institut für Kernphysik, Technische Universität Darmstadt, Schloßgartenstr. 9, 64289 Darmstadt, Germany
E-mail: c.omet@gsi.de

New Journal of Physics **8** (2006) 284
Received 12 June 2006
Published 28 November 2006
Online at http://www.njp.org/
doi:10.1088/1367-2630/8/11/284

Abstract. Intense heavy ion beams from the Gesellschaft für Schwerionenforschung (GSI-Darmstadt) accelerator facilities are investigated for their potential to drive inertial fusion targets and are currently used to generate and probe high-energy-density (HED) matter. The existing heavy ion synchrotron facility SIS-18 delivers intense uranium beam pulses for experiments with up to 4×10^9 ions per bunch at a charge state of $q = 73+$. Higher intensities are potentially available at lower charge states, when related loss mechanisms can be overcome. We have observed intensity-dependent beam losses in SIS-18. The origin of these beam losses is attributed to processes changing the charge state of ions, which is predominantly due to collisions with rest gas atoms. The resulting change in the mass over charge ratio m/q leads to modified trajectories in dispersive beam transport elements, and finally to the loss of the particle at the vacuum tube wall. At the impact position secondary particles are produced by ion-induced desorption and as a result the pressure in the vacuum tube is increased locally. This local rise in pressure in turn leads to increased charge changing processes starting an avalanche process that may eventually lead to a complete loss of the beam during a few turns in the synchrotron. In this paper, we discuss a method to control the problem of desorbed gases with specifically designed beam catchers at critical positions. We have further developed a program package to calculate the most important beam loss mechanisms and to couple them to the dynamic vacuum problem. The basis of this simulation is an ion–optics routine where relevant atomic processes and the effects of dynamic vacuum are implemented.

[3] Part of PhD Thesis of C Omet, Technische Universität Darmstadt, 2006.
[4] Author to whom any correspondence should be addressed.

PII: S1367-2630(06)26458-9

Contents

1. Introduction

The success of nuclear and particle physics of the past decades is intimately connected to the impressive development of accelerator physics and accelerator technology, which was striving forever increasing particle energies. A new trend is, however, observable. A number of applications call for very high beam intensities and beam power. One of these research fields is Inertial Fusion Energy (IFE), and an accelerator driver for this purpose may well be viewed as the ultimate challenge for accelerator physics, since the Inertial Confinement Fusion (ICF) scenario requires a total energy of a few MJ to be delivered into a beam spot of millimetre size, within a time range of approximately 10 ns.

Today heavy ion driven fusion in many respects is still a field of basic science issues. Existing accelerator facilities, which are predominantly built for nuclear and particle physics are used to address key issues of ion driven fusion (see [1]–[3]). The Gesellschaft für Schwerionenforschung (GSI) accelerator is one example for this concept [4]. Recently a proposal to build a new machine at GSI for antiproton and ion research has been approved [5]. Figure 1 shows the new accelerator together with the existing machine. The new accelerator consists of a heavy ion synchrotron, which actually is composed of two rings which are capable to produce ion beams with a magnetic rigidity of 100 and 300 Tm.

The new accelerator facility relies on the existing SIS-18 synchrotron as an injector. Currently most experiments which call for highest intensities are performed with a uranium

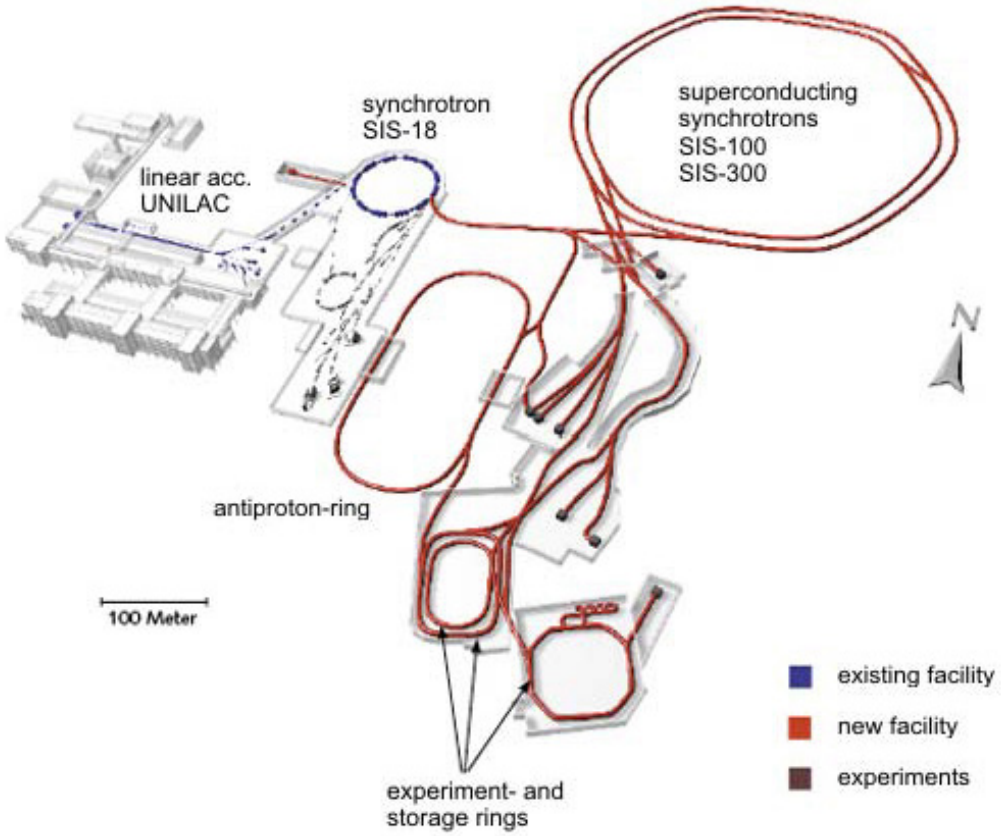

Figure 1. Layout of the new accelerator facility at GSI.

ion beam at a charge state of 73+. In a recent experiment to study properties of high-energy-density (HED) matter, a total number of 4×10^9 particles were transported to the target area in a bunch of approximately 120 ns focused to a sub-millimetre spot. Even higher intensities will be available using uranium ions with a charge state of $q = 28+$, and it is planned to fill the SIS-18 synchrotron up to the space charge limit of about 2×10^{11} particles at the injection energy of $11.4\,\mathrm{MeV\,u^{-1}}$.

To prove the feasibility, experiments at the SIS-18 were conducted to test high intensity uranium operation with low charge states. During these, a varying number of U^{28+}-particles up to 7.4×10^9 were injected and stored at the injection energy of $11.4\,\mathrm{MeV\,u^{-1}}$. The results (see figure 2) showed extremely fast and intensity-dependent particle losses. Fast pressure measurements, conducted at the same time, revealed a very dynamic behaviour of the residual gas pressure. These effects were observed at intensities far below the space charge limit of the machine. An explanation of these observations is the charge change of the beam particles, which influence the vacuum in connection with ion-stimulated desorption.

Therefore, a quantitative description of the observed effects, which affect the life time of intermediate charged ion beams need to include calculation of the interaction of the beam particles with rest gas molecules/atoms and particle trajectories with aperture limits in the ring structure. In the following, these effects and a method to reduce the losses are summarized.

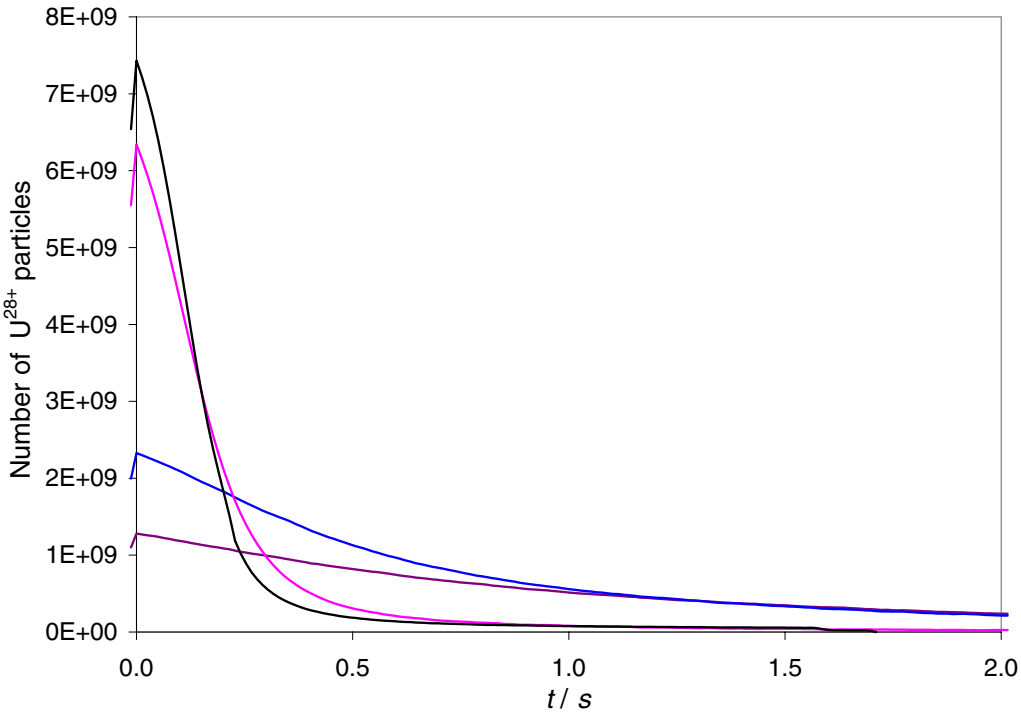

Figure 2. Measured intensity of a stored U^{28+}-beam in the SIS-18.

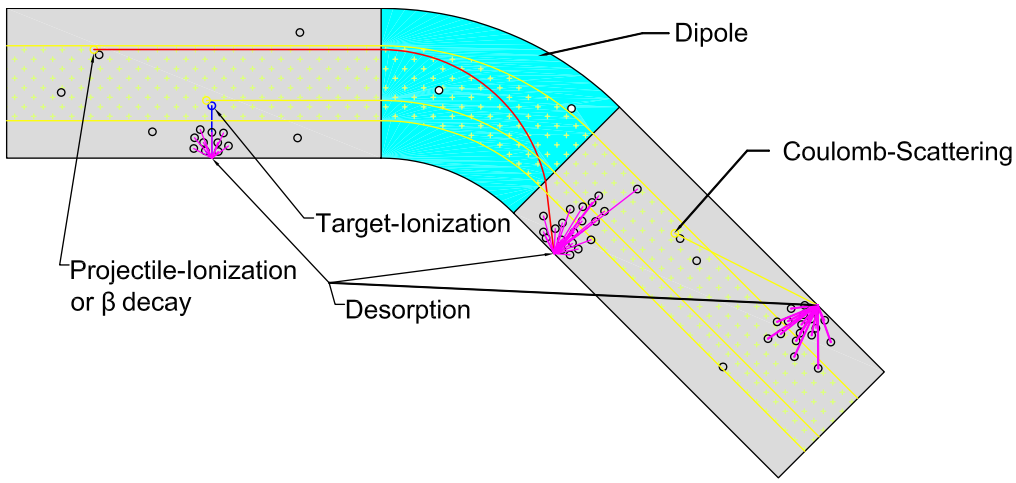

Figure 3. Beam loss processes and interaction with the residual gas in an accelerator.

2. Beam loss mechanisms

Particles of the circulating beam (projectiles) in the vacuum of a ring accelerator undergo several effects, which affect their storage time in the ring (see figure 3). The projectile ionization and eventually radioactive decay leads to a change of the particle's m/q ratio. In dispersive beam

transport elements, this results in a strong deviation of the trajectory in comparison to the reference ion. Similar to Coulomb scattering, this will lead usually to an impact at the vacuum tube or acceptance defining devices (depending on the machine's acceptance). For simplification, we do not take into account intra beam scattering, resonances caused by magnet errors or space charge effects at the moment.

All mentioned effects may lead to particles hitting the vacuum tube with high energies and therefore initiate there desorption of secondary particles which are loosely bound to the surface (the binding energy is usually a few eV). Two cases of ion-stimulated desorption have to be considered:

1. Ion impact under grazing incidence of the projectile ion with high projectile energy ($\gg$1MeV).
2. Impact of ionized rest gas molecules under nearly perpendicular angle of incidence with low energies (acceleration by the beam potential to a few keV).

The produced local gas cloud can be ionized and repeat the last process, but this is neglected due to simplification. Continuous pumping and outgassing of metal surfaces is resulting in an equilibrium vacuum pressure for all rest gas components. In the following, the effects are described in detail.

2.1. Projectile ionization

The heavy and fast beam ions are ionized by collisions with residual gas particles (which are virtually at rest). The charge exchange can occur either as electron loss or electron capture. The cross-sections for these effects in the typical energy range of modern accelerators ($\mathrm{MeV\,u^{-1}} \ldots \mathrm{GeV\,u^{-1}}$) have been measured only for a few ion species. For higher (but still non relativistic) energies, Olson *et al* [6] have calculated charge exchange cross-sections for U^{28+} in the order of $1 \times 10^{16} \ldots 1 \times 10^{-20}\,\mathrm{cm^2\,atom^{-1}}$. If one sums over all charge exchange cross-sections of all rest gas components, the charge exchange rate Γ_{PI} is given by

$$\Gamma_{\mathrm{PI}} = \beta c \sum_i n_i \sigma_i(E, q), \tag{1}$$

where β is the relativistic factor, c the speed of light, n_i the particle density of the rest gas component i and σ_i is the projectile energy (E) and charge state (q)-dependent charge exchange cross-section. The accelerator's momentum acceptance may be large enough, that particles with charge exchange survive several turns (this is the case especially in a storage ring or a synchrotron with a high tune).

2.2. Single Coulomb scattering by rest gas particles

Beam particles can be scattered by collisions with rest gas particles. Under the assumption, that bound electrons do not contribute to scattering, but to the energy loss [7], Madsen [8] has found that the beam loss rate for single Coulomb scattering Γ_{CS} can be described as

$$\Gamma_{\mathrm{CS}} = \frac{2\pi Z^2 r_{\mathrm{p}}^2 c n_{\mathrm{sc}}}{A^2 \gamma^2 \beta^3} \left(\frac{\langle \beta_x \rangle}{\epsilon_{\mathrm{acc},x}} + \frac{\langle \beta_y \rangle}{\epsilon_{\mathrm{acc},y}} \right), \tag{2}$$

where $r_p = 1.535 \times 10^{-18}$ m is the classical proton radius, $\langle\beta\rangle$ is the average beta function and ϵ_{acc} the acceptance of the accelerator. A is the mass number and Z the nuclear charge number of the ion. Finally, n_{sc} is the Coulomb scattering density, which is given by

$$n_{sc} = \sum_i Z_i^2 \cdot n_i, \tag{3}$$

where n is the particle density and Z the nuclear charge number of a particular vacuum component i. The loss rate for intermediate charged ions by Coulomb scattering in the typical energy range of an accelerator (MeV u^{-1} ... GeV u^{-1}) is three to four orders of magnitude lower compared to the loss rate by projectile ionization.

2.3. Radioactive decay

When accelerating radioactive nuclei for nuclear structure or neutrino experiments, e.g. a β-decay changes the charge state and momentum of a projectile ion. At high energies, the momentum over charge ratio $\Delta p/\Delta q$ deviation of the daughter product, caused by the energy change, is much smaller than the deviation caused by the charge state change. The loss rate by radioactive decay Γ_β is a purely statistical process and described by

$$\Gamma_\beta = \frac{1}{\gamma\tau} = \frac{\ln(2)}{\gamma t_{1/2}}, \tag{4}$$

where $t_{1/2}$ is the half-life time of the radioactive particle and γ the relativistic factor.

2.4. Summary of the loss mechanisms

If we summarize the above mentioned loss mechanisms, we find the total loss rate of the primary beam (projectile) Γ_P in the vacuum to be

$$\Gamma_P = \Gamma_{CS}(n_i, \beta) + \Gamma_{PI}(n_i, \beta) + \Gamma_\beta(\beta). \tag{5}$$

This equation can be rewritten in order to derive the time-dependent number of primary beam particles N (eventually consisting of different charge states j):

$$\dot{N}_j = -N_j \cdot \Gamma_P(n_i, \beta). \tag{6}$$

If one considers only static vacuum conditions ($n_i = \text{const.}$), the solution of (6) would be an exponential decay of the particle number. In order to make the calculation realistic, we have to introduce a dynamic vacuum behaviour in the next section.

3. Accelerator vacuum

To complete the description of the interaction between the beam and the residual gas, one has to take into account the target ionization and desorption process. Both are described in the following, then we can complete the formalism with the dynamic vacuum calculation.

3.1. Target ionization

The gas molecules (virtually at rest) can be ionized by the fast and heavy beam projectiles. This results in a free electron and an ionized rest gas molecule, which can be accelerated to the vacuum tube by the beam potential. There it will hit the vacuum tube under nearly perpendicular angle of incidence at energies of a few keV or less (depending on the beam space charge potential). The cross-section for the target ionization σ_{B} can be described by the well known Bethe formula [9]

$$\sigma_{\mathrm{B}} = 4\pi a_0^2 \frac{\alpha^2}{\beta^2}\left[M_i^2\left(\ln\frac{\beta^2}{1-\beta^2} - \beta^2\right) + C_i + \gamma_i\frac{\alpha^2}{\beta^2}\right], \tag{7}$$

where a_0 is the classical Bohr atom radius and α the fine structure constant. M_i, C_i and γ_i are target specific parameters, which were determined empirically in [9]. This formula is independent of the projectile's charge and mass. The sign of the charge state is only important at energies lower than $\approx$2 MeV u^{-1}. Then the collision is described in terms of the atoms as a whole, not only as a Coulomb collision of the target electrons with the projectile.

For particles with charge states $q > 1$, Gillespie [10] found that the target ionization cross-section σ_{TI} scales with

$$\sigma_{\mathrm{TI}} = q^2 \exp\left(-\lambda|q|\frac{\alpha^2}{\beta^2}\right)\sigma_{\mathrm{B}}, \tag{8}$$

where λ is an empirically determined target specific parameter. For common vacuum components, one can find these parameters in [11]. The ionized-molecule production rate by target ionization Γ_{TI} is

$$\Gamma_{\mathrm{TI}} = \beta c \sum_i n_i \sigma_{TI,i}(q). \tag{9}$$

3.2. Ion impact-induced desorption

If particles with a trajectory modified by the above mentioned effects are not strongly focused towards the beam axis, they will hit the vacuum tube under grazing incidence (or they will hit acceptance limiting devices under nearly perpendicular angle of incidence). Molecules, attached loosely to the wall's surface are then desorbed at calculated rates of $\eta_\angle \approx 5 \times 10^3 \ldots 30 \times 10^3$ molecules ion^{-1} [12]. Other calculations at the Relativistic Heavy Ion Collider (RHIC) at the Brookhaven National Laboratory (BNL) [13] estimated desorption rates of up to $\eta_\angle \approx 10^6$ at higher energies. Since this parameter is not well known and changes a lot with surface treatment, it is left open and estimated by fitting to measurement results.

Ionized-rest gas molecules accelerated by the beam potential will hit the vacuum tube under nearly perpendicular angle of incidence with energies of a few keV or less, as stated before. This leads to moderate desorption rates in the range of $\eta_\perp \approx 1, \ldots, 10$ (see [14]).

The ion-stimulated desorption effect is not easily reducible by means of surface treatment (e.g. an Ar-glow discharge-treated surface would contain a lot of Ar, which can easily be desorbed). Investigations at the BNL [15] have shown that the desorption rate depends on the electronic energy loss $(\mathrm{d}E/\mathrm{d}x)^2$ of the ion in a given material. Since the physics behind the desorption effect itself is not understood in all details, further investigations of the Ultra High Vacuum (UHV) group at the desorption test stand at GSI have shown that blank, polished copper or silicon surfaces have a very low desorption rate. No material with a zero desorption rate has been found so far.

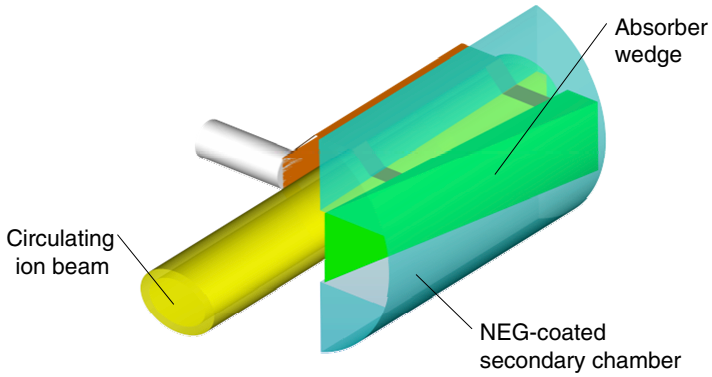

Figure 4. Design concept of a desorption gas controlling ion catcher.

3.3. Dynamic vacuum stabilization concepts

The new synchrotron design concept developed for the SIS-100 in the FAIR project is based on residual gas pressure stabilization by means of a dedicated ion catcher system and strong pumping of cold surfaces. A properly designed system of catchers must control most of the ionized or scattered particles, before they reach the vacuum pipe and generate desorption gases. Furthermore, the catcher system should not reduce the acceptance of the machine. This can be achieved by a properly designed lattice cell and positioning of the catchers [16].

Investigations of the ion-stimulated desorption effect using Elastic Recoil Detection Analysis (ERDA) technology are conducted at GSI. As mentioned before, no material with a desorption rate of $\eta \approx 0$ has been found. Thus a properly designed collimator should confine the produced desorption gases, so that they are prevented from reaching the beam axis (and produce more charge exchange there). Such a system was proposed in [17].

In order to control the charge change-generated beam losses and the produced desorption gases, one can consider a solution by a properly designed catcher system as shown in figure 4. It uses a wedge-shaped beam absorber on which the desorption gases are produced at the side of the wedge pointing away from the main beam. The desorption gases can be pumped away quickly by a Non Evaporable Getter (NEG)-coated surface, before they reach the beam axis again. For a successful installation, the positions of the beam impacts on to the vacuum chamber must be known. The deviation of the m/q ratio of a particle with a different charge state q compared to the reference ion with the charge state q_0 is equivalent to a momentum deviation $\Delta p/p$ of

$$\frac{\Delta p}{p} = \frac{q_0}{q} - 1. \tag{10}$$

The calculation of the impact position can be determined via linear beam optics, following the description given in textbooks as [18, 19]. To each ion optical element, a transfer matrix is assigned, which can be applied to particles with momentum deviation, too. Elements with higher order effects (e.g. sextupoles) can be described by other algorithms (e.g. like a kick).

3.3.1. Efficiency of a catcher system. Under the assumption of a smooth pressure distribution, the probability of charge exchange processes is distributed homogeneously over the accelerator's circumference. Figure 5 shows the predicted trajectories of the charge exchange $U^{28+} \rightarrow U^{29+}$

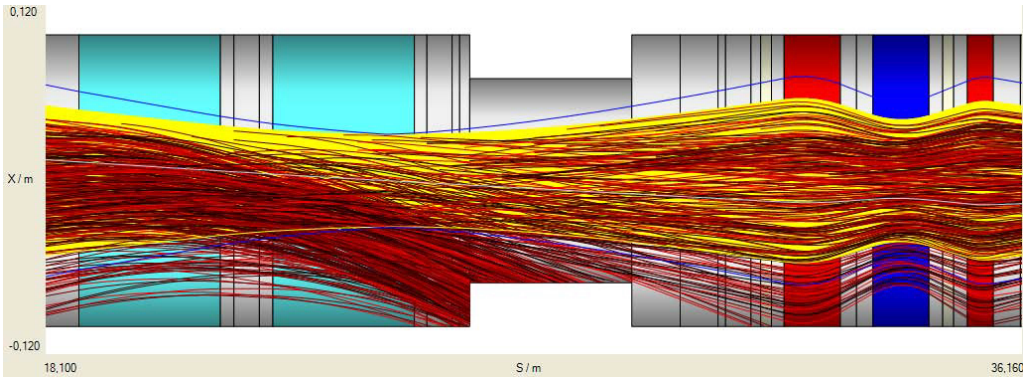

Figure 5. Calculated trajectories of $U^{28+} \rightarrow U^{29+}$ in the horizontal plane of SIS-18 section S02. Dipoles are cyan, quadrupoles in red/blue and the U^{28+}-envelope in yellow. Note the step in aperture in the RF cavity.

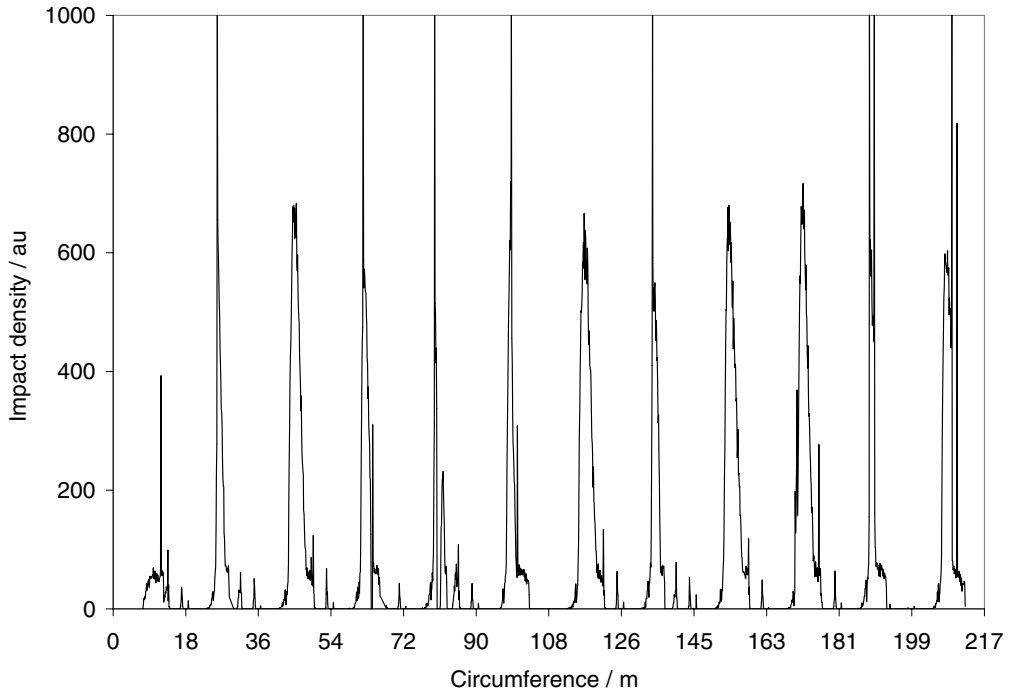

Figure 6. Calculated impact distribution of $U^{28+} \rightarrow U^{29+}$ in SIS-18.

in one section of SIS-18, whereas figure 6 shows a histogram of the impact intensities along the whole circumference. The peaks are situated after the dipoles in each lattice cell. In order to reduce impacts on the wall efficiently, the catchers should be situated 'upstream' of the positions with high impact probabilities.

For a detailed analysis of the quality of a catcher system, the number of particles hitting the catchers N_c and the wall N_w defines the catching efficiency θ with

$$\theta = \frac{N_c}{N_w + N_c}. \tag{11}$$

Table 1. Vacuum parameters.

Parameter	Unit
Equilibrium pressure p_0	Pa
Equilibrium vacuum components $p_{i,0}$	%
Components of the desorption gas D_i	%
Effective pumping speed S	$m^3\ s^{-1}$
Temperature T	K

Generally, the catching efficiency turns out to be a function of the beam emittance as well as a function of the machine's acceptance, the beam energy and the position of the catchers.

3.4. Dynamic vacuum calculation

The key parameters for the calculation of the residual gas pressure dynamics in synchrotrons or storage rings are summarized in table 1. The dependence of the pumping speed on the residual gas pressure is neglected for the moment. Other parameters such as volume, surface, etc. can be extracted from the lattice and catcher geometry. It is sufficient to assume an averaged pressure because all mentioned loss mechanisms are linear in pressure.

Finally, the time-dependent density of each vacuum component i is given by

$$\dot{n}_i = -\dot{N}_j[\eta_{\angle,i}\,(1-\theta(E,q)) + \eta_{c,i}\theta(E,q)] + \eta_{\perp,i}\Gamma_{TI}(n_i,\beta) + Q_{i,o} - Q_{i,p}, \tag{12}$$

where η_c is the desorption rate of the catcher system, Q_o the outgassing rate and Q_p the effective pumping rate of the vacuum system.

Equations (6) and (12) describe a system of coupled differential equations, which is in general not easily solvable (β and E are time dependent during acceleration). However, solving this system by numerical methods (e.g. by Euler's method with a time increment $\Delta t = T_{turn}$) is comparably easy.

All above mentioned loss mechanisms are linear in pressure; therefore it is correct to neglect the spatial dependency. This is not the case for the calculation of the catching efficiency because the vacuum pressure and therefore the charge exchange process is not uniformly distributed along the circumference. To consider this effect, one has to calculate a spatially resolved pressure profile, which is described in the following.

3.5. Spatially resolved pressure calculation

For an exact estimation of the catcher efficiency, a longitudinal resolved pressure distribution is needed. Only a few vacuum calculation codes do exist for the pressure range of interest (UHV, i.e. $p < 1 \times 10^{-7}$ mbar), e.g. VAKTRAK [20] or VAKDYN [21]. Most of them add vacuum conductance values for a given lattice. As shown in [22], this assumption is wrong in some cases. The algorithms become numerically unstable at extreme pumping speeds, very low pressures or very small conductance values. To overcome these problems, the Monte Carlo algorithm given in [23] is summarized as follows.

The vacuum pressure in ring accelerators is typically in the regime of molecular flow, e.g. the typical dimensions of vacuum tubes d is small compared to the mean free path length of rest

gas molecules $\lambda \gg d$. One can calculate the pressure distribution by using the convenient way of describing an ion–optics lattice by n short elements.

The calculation is launched by a particle, which is thermally desorbed out of a surface with a *cos*-distribution around the surface normal. Then the path of the molecule under observation is tracked by a simple raytracing algorithm, until it reaches a pump (or pumping surfaces, respectively). The resulting path length is stored in a matrix $\langle S_{ij} \rangle$, where each matrix element describes the mean free path length of a molecule in a lattice element j, which was produced in the lattice element i. For a Maxwell–Boltzmann–distribution the average reciprocal molecular speed $\left\langle \frac{1}{v} \right\rangle$ is given by

$$\left\langle \frac{1}{v} \right\rangle = \frac{4}{\pi \overline{c_{\mathrm{G}}}}, \tag{13}$$

where $\overline{c_{\mathrm{G}}}$ is the average molecular speed, given by

$$\overline{c_{\mathrm{G}}} = \sqrt{\frac{8 k_{\mathrm{B}} T_{\mathrm{G}}}{\pi m}}, \tag{14}$$

where k_{B} is the Boltzmann constant, T_{G} the gas temperature and m the molecule's mass. With (13), the average residence time τ of a molecule in lattice element j, which was produced in lattice element i is given by

$$\langle \tau_{ij} \rangle = \left\langle \frac{1}{v} \right\rangle \langle S_{ij} \rangle = \frac{4}{\pi \overline{c_{\mathrm{G}}}} \langle S_{ij} \rangle. \tag{15}$$

The absolute number of molecules in element j, which were produced by thermal outgassing with the rate $\dot{N}_i$ in Element i, therefore is

$$N_{ij} = \dot{N}_i \langle \tau_{ij} \rangle. \tag{16}$$

Finally, the molecules do not interact with each other, so the number density in one element is given by superposition of the thermal outgassing in all elements

$$n_j = \frac{1}{V_j} \sum_i \dot{N}_i \langle \tau_{ij} \rangle. \tag{17}$$

The calculation of the pressure profile is therefore reduced to a simple molecular raytracing through the ion–optic elements. As the lattice is constant, one has to calculate the $\langle S_{ij} \rangle$-matrix only once, which is an advantage for repeated calculations. An example of the pressure profile calculation by this algorithm is shown in figure 7. The thermal outgassing rate was assumed to be $\dot{N} = 4 \times 10^{-12}\,\mathrm{mbar\,l/(s\,cm^2)}$, which is a common value for stainless steel. The measured data agrees quite well with the simulation in all but in two positions which is due to the fact that the SIS-18 is not a closed ring, but has injection and extraction channels. These were excluded from the calculation.

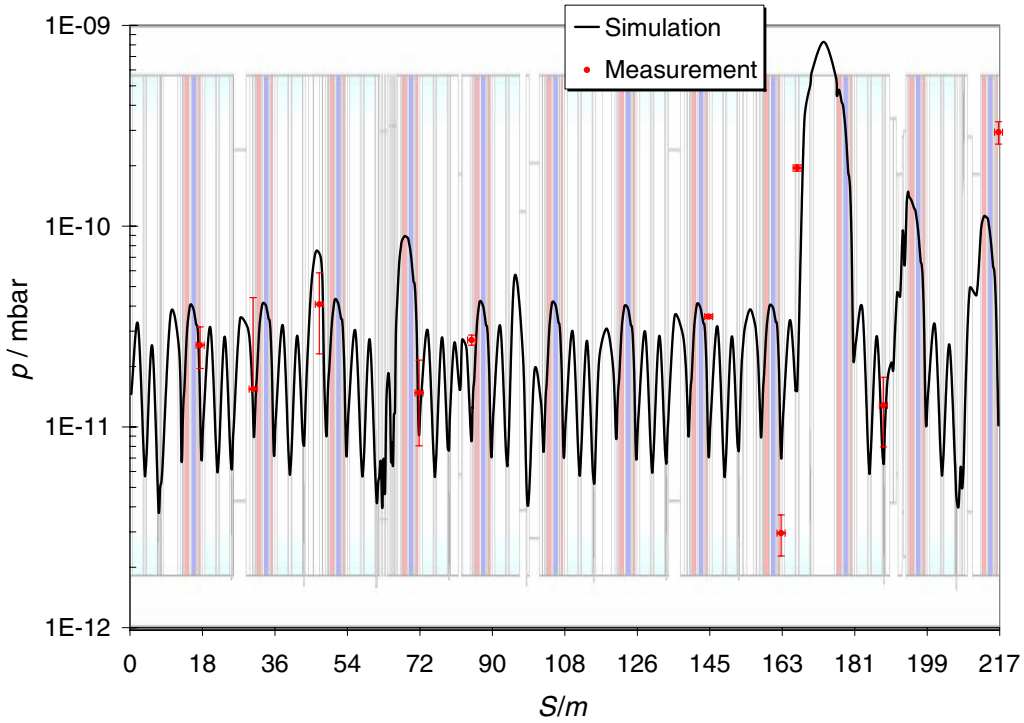

Figure 7. Calculated longitudinal pressure profile in the SIS-18.

4. Synchrotron cycle

To complete the quantitative description, all characteristic phases of a synchrotron's acceleration cycle should be accounted for with their typical systematic losses. For example, the beam current during a multi turn injection process is continuously rising, whereas it is rising stepwise in case of a bunch to bucket stacking. Fast and slow extraction have other characteristic loss mechanisms (such as systematic losses).

The different phases of a synchrotron cycle are shown in figure 8. During all these phases, systematic losses can occur, especially at injection by filling an already occupied volume of the phase space or mismatch during the RF-capture process.

5. Simulation code 'STRAHLSIM'

All above mentioned effects like Coulomb scattering, projectile and target ionization, radioactive decay, desorption, outgassing, pumping, longitudinally resolved pressure calculation, acceleration cycle and the ion optics have been implemented in the program package 'STRAHLSIM'. All parts of the program were written in the language C#. The Graphical User Interface (GUI) runs on every PC with .NET Framework CLR installed (currently Windows or Linux) and uses automatically all processors available.

For the most common vacuum components (H, C, N, O, Cl and Ar) and certain projectiles (U^{10+} from [24], U^{28+} from [6], U^{73+} from [25], Pb^{54+} from [11] and Au^{32+} from [26]), calculated or measured charge exchange cross-sections do exist in different energy ranges. These data

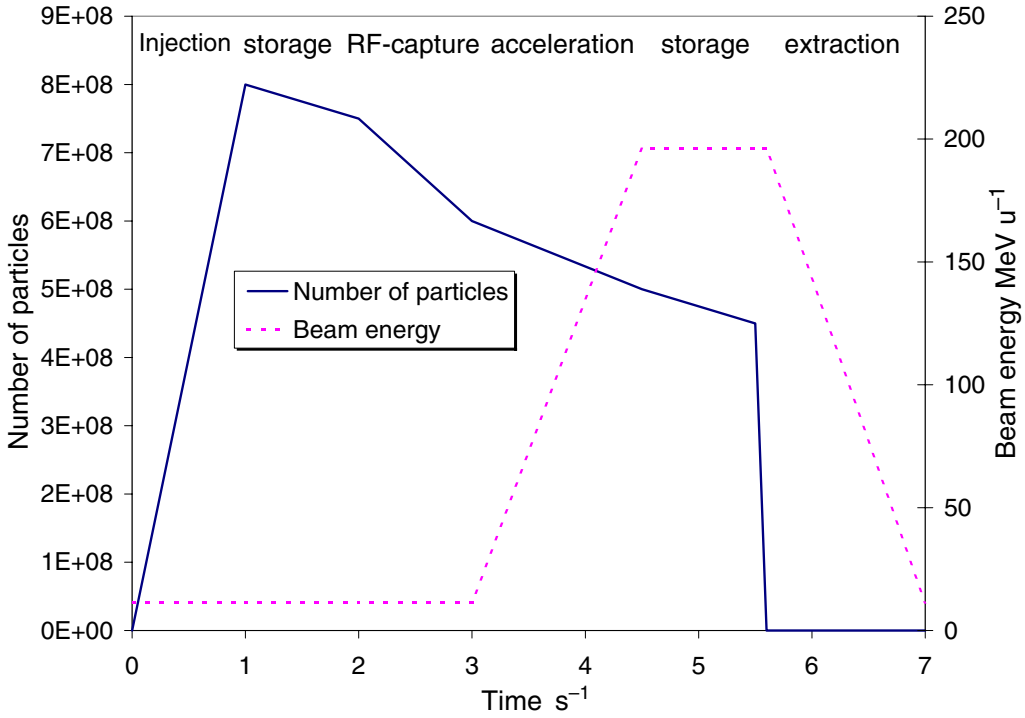

Figure 8. Schematic plot of the beam intensity over a typical acceleration cycle with various types of systematic beam losses.

are read into the program from a text file. Missing data in the energy dependence are inter-/extrapolated via exponential functions from this data.

Presently implemented ion optical elements are drift spaces, dipoles (rectangular or bend, both with edge angles), quadrupoles, combined function magnets (dipole and quadrupole), sextupoles and wedge-shaped catchers. For all optical elements apertures can be defined (this is not the case for the commonly used ion–optic codes MAD-X [27] and MIRKO [28]). Elliptical or rectangular cross-sections (both with offsets relative to the optical axis) can be chosen.

The beam envelopes, calculated with 'STRAHLSIM' were compared and agree with the codes MIRKO and WinAGILE [29]. All properties of each element can be directly changed via the GUI. An import and export of WinAGILE, MIRKO and AML (Accelerator Markup Language, a XML-structure [30]) data files is possible, to MAD-X file format only an export is currently implemented.

Initial beam parameters are entered in x (horizontal) and y (vertical) direction as TWISS parameters in the phase-space. At present, two distribution functions for the beam are supported (both cut hard at the 2-σ k-v-edge): Bi-Gaussian and rectangular. The selected tune and incoherent tune shift after injection can be displayed together with the systematic resonance lines in a simple tune diagram.

The program is able to distribute the catchers automatically over longitudinal positions (determined by the element's name). The transverse position can be varied over a certain range (in units of the beam width at place of the catchers).

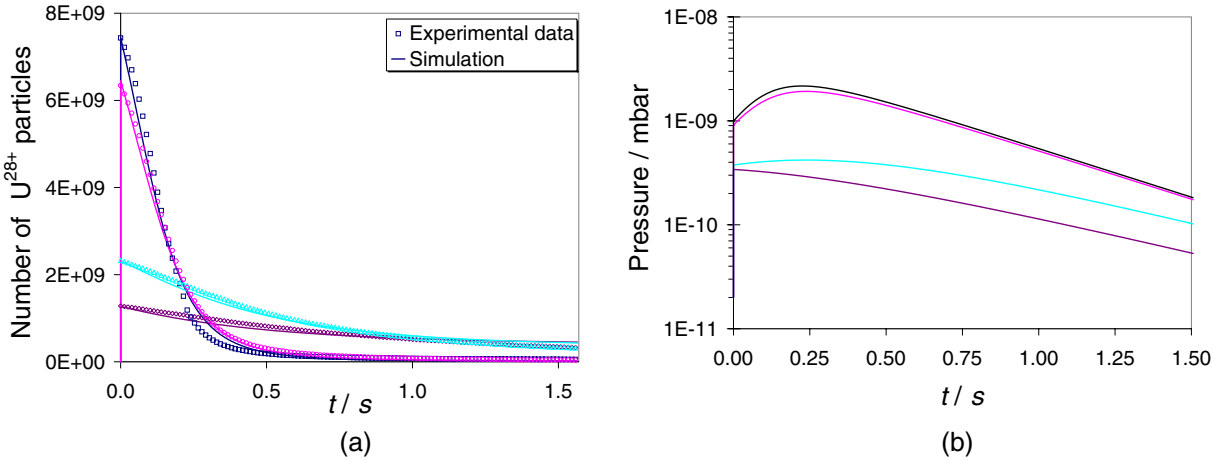

Figure 9. Measured and calculated number of U^{28+}-particles and calculated pressure in the SIS-18. Note: All parameters but the number of injected particles were kept constant.

6. Benchmarking and applications

Originally, STRAHLSIM has been developed for the intermediate charge state, heavy ion beam operation (e.g. U^{28+}) in the SIS-18 and SIS-100 for the FAIR project. The verification of the physics model was performed by comparing simulations with the experimental data mentioned in the introduction. A very good agreement with the experimental data was achieved, as shown in figure 9. The pressure rise due to injection losses is very large. However, meanwhile the code was extended and applied to several other machines and projects elsewhere.

6.1. SIS-18 upgrade

The SIS-18 will be upgraded [31] for highest beam currents required for the FAIR project [5]. The dynamics of the residual gas pressure was simulated with STRAHLSIM. To minimize the losses in SIS-18 during acceleration, simulation showed that beside the equilibrium pressure of the XHV-system, the injection losses of the multi turn injection, a large distributed pumping speed and an effective catcher system are most critical.

Especially the injection losses produce a very high pressure bump in the range of several orders of magnitude during a few μs, which has to be pumped quickly. For this purpose, a NEG coating of the dipole and quadrupole chambers is foreseen. This should deliver a distributed pumping speed, which is a factor of 100 higher than the currently installed.

In addition, a dedicated catcher system for the U^{28+} operation will be installed to control the charge change-generated beam losses at high current operation and confine the desorbed gases.

6.2. SIS-100 lattice design

A new lattice design concept has been developed for the SIS-100 [32]. Each cell in the SIS-100 lattice has been designed as a charge separator for the charge state 29+ of the reference ion U^{28+} (see figure 10; a high fraction of U^{29+} is kept temporarily in the acceptance and will be scraped off

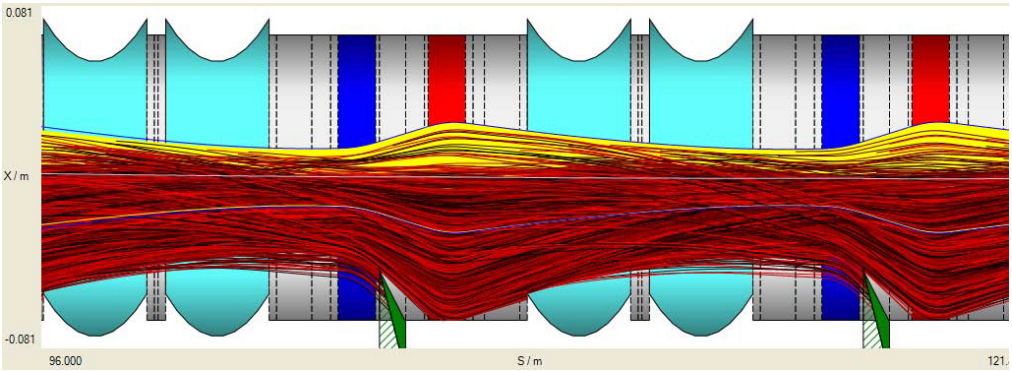

Figure 10. Plot of the SIS-100 lattice in the horizontal plane showing catchers and trajectories for $U^{28+} \rightarrow U^{29+}$.

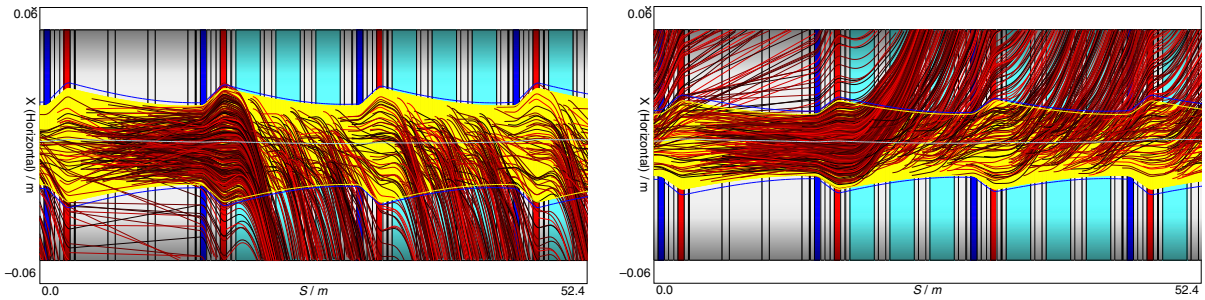

Figure 11. Trajectories in the horizontal plane of radioactive decay products $^{6}He^{2+} \rightarrow {}^{6}Li^{3+}$ (figure 11(a)) and $^{18}Ne^{10+} \rightarrow {}^{18}F^{9+}$ (figure 11(b)) in the proposed PS replacement lattice G7.

a few turns later). The catchers are positioned that the acceptance of the machine is not affected. It turned out that the commonly used FODO and triplet focusing structures are not well suited for this kind of optimization, because a beam waist cannot be achieved at every position of good separation of U^{29+}.

6.3. Beta beams

Within the framework of the beta beams project [33], beam loss and pressure evolution calculations for the CERN PS, SPS and the planned RCS were done. A new lattice for the PS was proposed by the GSI study group [34] to generate a peaked-loss distribution of the radioactive decay products with maximums in between the magnets (see figure 11). This was done to protect the PS magnets from impact of the beta beam decay products.

In figure 12(a), the calculated time evolution of the stacking process and number of stored and lost radioactive $^{6}He^{2+}$ particles in the CERN PS is shown. It is shown in figure 12(b), that a stabilization of the dynamic vacuum pressure to values below 1×10^{-8} mbar is possible with a pumping speed enhancement of a factor 16.

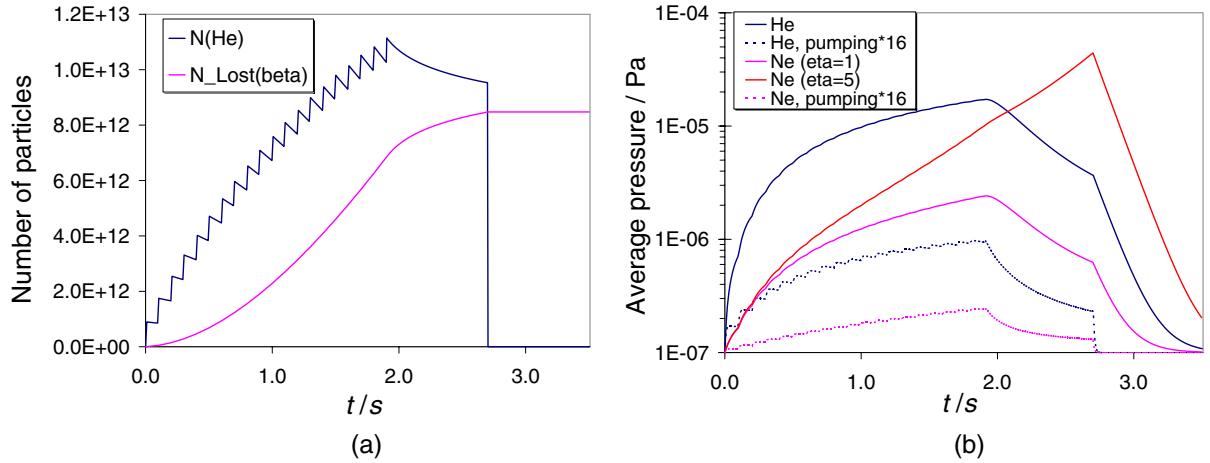

Figure 12. Number of particles of a radioactive $^{6}He^{2+}$-beam and pressure evolution in the CERN PS during operation with β-beams.

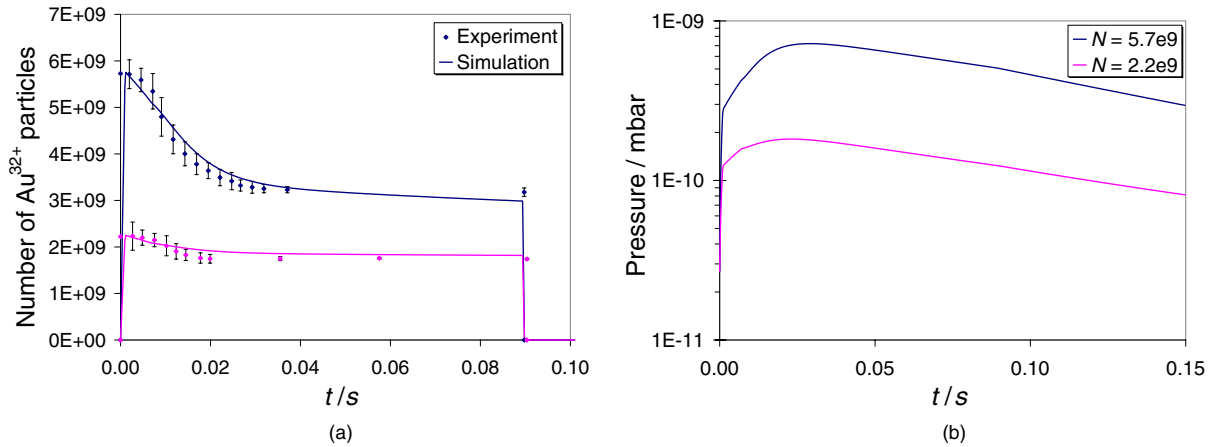

Figure 13. Measured and calculated number of Au^{32+} particles and pressure evolution in the AGS Booster.

6.4. AGS booster

The beam loss during the AGS booster operation with low charge state heavy ions (Au^{32+}) was calculated (STRAHLSIM simulation with measurements, see figure 13). It was shown that the current operation with 5.7×10^{9} Au^{32+} particles is at the intensity limit of that machine [35], what is similar to the present operation of SIS-18 with U^{28+}.

7. Summary and limitations

The program 'STRAHLSIM' was developed to simulate beam losses in synchrotrons, operated at high intensities with intermediate charged heavy ions. The basic processes underlying these beam losses are charge exchange and desorption effects, generating a dynamic vacuum behaviour. Furthermore, the program has the ability to estimate the vacuum limited intensity border of current machines and to find appropriate measures to overcome this limit.

Nonlinear and collective effects such as space charge or resonances were not taken into account so far. Due to a lack of experimental data, charge exchange cross-sections are extrapolated and therefore uncertain at very high energies.

References

[1] Neff S, Knobloch R, Hoffmann D H H, Tauschwitz A and Yu S S 2006 *Laser and Particle Beams* **24** 71–80
[2] Tahir N A *et al* 2004 *Laser and Particle Beams* **22** 485–93
[3] Tahir N A *et al* 2003 *Phys. Rev. Special Top.* **6** 020101
[4] Hoffmann D H H *et al* 2005 *Laser and Particle Beams* **23** 47–53
[5] Henning W F 2004 *Nucl. Instrum. Methods Phys. Res.* B **214** 211–5
[6] Olson R E, Watson R L, Horvat V, Perumal A N, Peng Y and Stöhlker T 2004 *J. Phys. B: At. Mol. Opt. Phys.* **37** 4539–50
[7] Jackson J D 1975 *Classical Electrodynamics* 2nd edn (New York: Wiley)
[8] Madsen N 1999 Beam evolution in the Antiproton Decelerator (AD) under the influence of residual gas and intra beam scattering *Note* PS/DI/Note 99-06, AD Note 047 CERN
[9] Rieke F and Prepejchal W 1972 *Phys. Rev.* A **6** 1507–19
[10] Gillespie G H 1983 *Phys. Lett.* A **93** 327–32
[11] Madsen N 1999 Vacuum changes during accumulation of Pb54+ in LEIR *Note* PS/DI 99-21 CERN
[12] Mustafin E, Boine-Frankenheim O, Hofmann I, Reich-Sprenger H and Spiller P 2003 *Nucl. Instrum. Methods Phys. Res.* A **510** 199–205
[13] Zhang S Y 2004 High intensity and high brightness hadron beams *AIP Conf. Proc.* **773** pp 216–8
[14] Boine-Frankenheim O, Krämer A and Rumolo G 2004 High intensity and high brightness hadron beams *AIP Conf. Proc.* **773** 229–32
[15] Molvik A W, Cohen R H, Bieniosek F, Friedman A, Covo M K, Lunda S M, Seidl P A, Stoltz P and Vay J L 2005 Electrons and gas versus high brightness ion beams, online at http://www-library.lbl.gov/docs/LBNL/573/52/PDF/LBNL-57352.pdf
[16] Spiller P, Blasche K, Franczak B, Kirk M, Hülsmann P, Omet C, Ratschow S and Stadlmann J 2005 *Nucl. Instrum. Methods Phys. Res.* A **544** 117–24
[17] Spiller P 2002 Vorschlag für einen Kollimatorpumpstand zur gezielten Beseitigung von Desorptionsgasen *Internal Note* GSI-SIS18-02-02 GSI
[18] Wille K 1992 *Physik der Teilchenbeschleuniger* (Wiesbaden: Teubner Verlag)
[19] Wollnik H 1987 *Optics of Charged Particles* (New York: Academic)
[20] Ziemann V 1992 Vacuum tracking *Tech. Rep.* SLAC-Pub-5962 (Stanford, CA: SLAC)
[21] Ziemann V 2006 Dynamic vacuum, online at http://www3.tsl.uu.se/∼ziemann/vakdyn/
[22] Oatley C W 1957 *Br. J. Appl. Phys.* **8** 15
[23] Bowden G B 2002 RF accelerator pressure profile by Monte Carlo *Linear Collider Collaboration Tech Note* SLAC-TN-03-055, LCC-0078 (Stanford, CA: SLAC)
[24] Olson R E, Watson R L, Horvat V, Zaharakis K E, Dubois R D and Stöhlker T 2005 *Nucl. Instrum. Methods Phys. Res.* A **544** 333–6
[25] Smolyakov A and Spiller P 2005 Electron capture for fast U73+ ions in gas targets. Application of Schlachter scaling rule at nonrelativistic energies *Internal Note* ACC-note-internal-2006-001 GSI
[26] Smolyakov A, Omet C and Spiller P 2005 Electron capture for fast ions in gas targets. Application of Schlachter scaling rule at nonrelativistic energies *Internal Note* ACC-note-2006-001 GSI
[27] Schmidt F and Grote H 2003 MAD-X—An upgrade from MAD8, CERN-AB-2003-024 ABP
[28] Franczak B 1984 *MIRKO—An Interactive Program for Beam Lines and Synchrotrons* (Berlin: Springer) chapter MIRKO
[29] Bryant P 2005 WinAGILE—Windows Alternating Gradient Interactive Lattice Design, online at http://bryant.home.cern.ch/bryant/

[30] Sagan D 2005 AML—Accelerator Markup Language, online at http://www.lns.cornell.edu/~dcs/aml/
[31] Spiller P, Blasche K, Hülsmann P, Krämer A, Ramakers H and Reich-Sprenger H 2004 *Proc. EPAC* pp 1180–1182
[32] Spiller P, Blasche K, Franczak B, Stadlmann J and Omet C 2004 High intensity and high brightness hadron beams *AIP Conf. Proc.* **773** 40–4
[33] Kirk M, Omet C, Spiller P and Stadlmann J 2005 Loss analysis for beta beam operation in existing CERN synchrotrons, unpublished
[34] Kirk M, Omet C, Spiller P and Stadlmann J 2005 Proposal for a replacement of the CERN PS with optimized collimation, unpublished
[35] Smolyakov A, Fischer W, Omet C and Spiller P 2005 Comparison of the present and planned operation of the SIS18 and the AGS booster with intermediate charge state heavy ions, GSI-Acc-Report-2005-11-001